An Immobilized (Carbene)Nickel Catalyst for Water Oxidation

Zhiyao Lu,[a] Debanjan Mitra,[a] Sri R. Narayan,[a] and Travis J. Williams*[a]

[a] *Donald P. and Katherine B. Loker Hydrocarbon Institute, Wrigley Institute for Environment and Sustainability, and Department of Chemistry, University of Southern California, Los Angeles, California, 90089-1661, United States.*

* Corresponding author
E-mail: travisw@usc.edu (T. J. Williams)

Dedication: To Pete Wolczanski, on the occasion of his 70th birthday, for helping us see simplicity in complexity; and in memory of the late Sri Narayan, who like Pete, never took his eyes off the details.

Keywords
OER, nickel, carbene, water splitting

Abstract
The oxygen evolution reaction (OER) of water splitting is essential to electrochemical energy storage applications. While nickel electrodes are widely available heterogeneous OER catalysts, homogeneous nickel catalysts for OER are underexplored. Here we report two carbene-ligated nickel(II) complexes that are exceptionally robust and efficient homogeneous water oxidation catalysts. Remarkably, these novel nickel complexes can assemble a stable thin film onto a metal electrode through poly-imidazole bridges, making them supported heterogeneous electrochemical catalysts that are resilient to leaching and stripping. Unlike molecular catalysts and nanoparticle catalysts, such electrode-supported metal-complex catalysts for OER are rare and have the potential to inspire new designs. The electrochemical OER with our nickel-carbene catalysts exhibits excellent current densities with high efficiency, low Tafel slope, and useful longevity for a base metal catalyst. Our data show that imidazole carbene ligands stay bonded to the nickel(II) centers throughout the catalysis, which allows the facile oxygen evolution.

1. Introduction

The oxygen evolution reaction (OER, 2 $H_2O \rightarrow 4\ H^+ + 4\ e^- + O_2 \uparrow$) of water splitting remains a central challenge in solar energy storage due to the slow and inefficient four-electron transfer process.[1] The search for an efficient and cost-effective water oxidation catalyst (WOC) presents two significant challenges: (1) OER usually requires highly oxidative conditions, under which many catalysts are easily decomposed;[2] (2) the catalyst must be based on abundant materials to meet global deployment demand. To solve these problems, the community has pursued new catalyst development with first-row transition metal complexes bearing inexpensive ligand sets.[3] Meaningful progress has been made in recent years in devising WOCs based on copper,[4] manganese,[5] iron,[6] and cobalt[7] complexes. Rather curiously, although nickel oxide is a leading commercial heterogeneous WOC, homogeneous nickel complexes for OER is less explored.[1-3, 8]

2. Results and Discussion

2.1. Catalyst Design and Discovery

Our search for efficient OER systems comprised a combination of 1) chemical homogeneous catalysis and 2) electrochemical heterogeneous catalysis. We focused on metal-carbene complexes for OER,[9] as we were intrigued by our lab's finding that metal-carbene complexes show much more flexible redox properties compared to their carbene-free congeners,[10] particularly on nickel,[11] and by the literature reports that a metal-carbene design can promote catalyst longevity in OER.[12] In our hands, iridium complex **1**[10defg] and nickel complexes **2** and **3** (Figure 1)[11] stay active for hours for water oxidation at a uniform rate in the presence of cerium ammonium nitrate (CAN, method see supporting information). When the loading of catalyst **2** is doubled at 50 °C, gas formation doubles proportionally, consistent with saturation catalysis by a single nickel species. Our focus gravitated toward these nickel complexes, because they present a promising solution to OER using an abundant, inexpensive material. The catalytically active nickel species persist under those harsh conditions employing concentrated CAN, as we observe linear kinetics throughout more than 1000 turnovers, or 50% conversion of CAN. Furthermore,

homogeneous nickel-carbene complexes can catalyze OER with remarkable activity under both chemical conditions and electrolysis, if immobilized onto an electrode surface. Designing such well-defined molecular catalysts that are stably bound to an electrode surface is exceedingly challenging; successful examples are rare.[13] Our nickel catalysts seem to bind the surface through one or more interactions to metal electrode in a way that is available both for nickel and platinum substrates. We expect this is happening through the ligand's imidazole ligand's nitrogen atoms. To the best of our knowledge, this is the first example of stably-surface-bound base-metal catalyst that originated from designs at the molecular level. This feature enlightens the possibilities to adopt new reactivities or novel mechanisms from homogeneous studies, and the opportunities to attune the reactivity and functionality of heterogeneous catalysts at an unprecedented level of control.

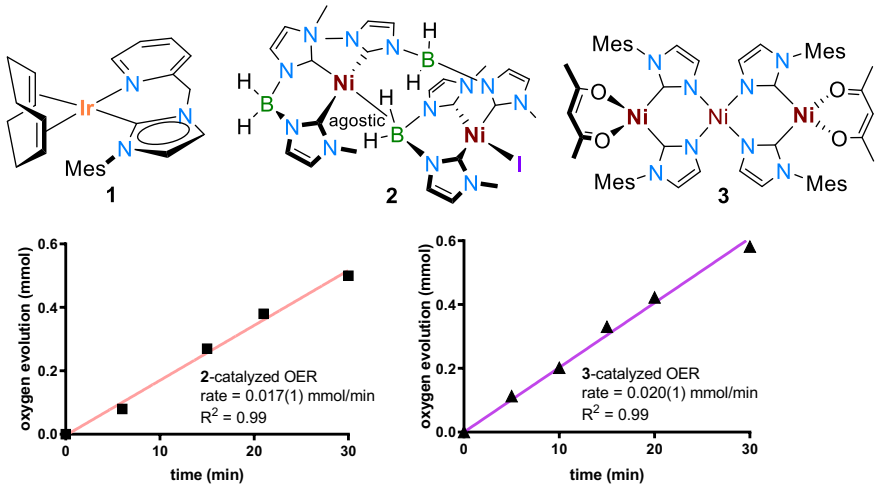

Figure 1. Carbene-supported precursors **1**, **2**, and **3** and the kinetic profile of an OER catalyzed by Ni complex **2** and **3** for the first 50% conversion of CAN. Reaction condition: 1.0 mg of nickel complex **2** (or molar equivalent of 3), 2 mL deionized H_2O, 2.0 g CAN, 70 °C. CCDC 1438246, 1455844, and 1455845 respective contain supplemental crystallographic details for compounds **1**, **2**, and **3**.

2.2. Chemical Water Oxidation

Homogeneous OER reactivity of complexes **1**, **2**, and **3** was examined by treatment of each with an aqueous solution of ceric ammonium nitrate, which is known to evolve O_2 cleanly in the presence of an appropriate catalyst.[14] The results are summarized in Table 1. We observe that

carbene-supported complexes **1**, **2**, and **3** all exhibit markedly better stability during OER than their synthetic precursors. For example, under our conditions, iridium complex **1** delivers 325 turnovers in 30 minutes, while $[Ir(COD)Cl_2]_2$ solution is deactivated immediately upon treatment with concentrated CAN (compare Table 1, entries 1 and 2). This contrast, as well as literature examples,[12ab] show that carbene ligands enhance the complex's stability against oxidative decomposition by CAN. Similarly, nickel complexes **2** and **3**, each featuring bidentate carbene ligands, are capable of more than 10^3 turnovers under chemical OER conditions, which places them among the most robust homogeneous base-metal water oxidation catalysts.[1, 6b]

While CAN is well known selectively to generate O_2 from aqueous solutions,[14] we took several measures to ensure that kinetic data quantified by formation of product gas are reliable. This reaction has known background photochemical reactivity, so we (1) protect all CAN reactions from light and (2) control against background rate, by subtracting the (typically zero) rate of a metal-free control reaction run on the same batch of reagents (see experimental section). Further, the fluid in the eudiometer is water, which traps CO_2, NH_3, or HCl gasses, should they evolve from the reaction. No pH deviation in the water was observed over continued use, indicating the absence of these materials.

The direct synthetic precursor of complexes **2** and **3** ($Ni(acac)_2$), the imidazole ligands, or a mixture of both do not exhibit any OER activity (Table 1, entries 5-7). We regard complexes **2** and **3** as pre-catalysts, because they convert to nickel-carbene species such as **6** in aqueous solutions through cleavage of the $–BH_2–$ group in **2** or the homoleptic central nickel atom in **3** (Scheme 1).[11] We find that the active OER catalysts are most likely homogeneous nickel-carbene species rather than metal oxide particles, because 1) we control the conditions so that cerium oxide particles do not form from thermolysis or photolysis;[13, 15] 2) the chemical OER's kinetic profiles are fast and linear at neutral pH, which is not appropriate for nickel hydroxide catalysts or for a simple nickel salt, regardless of whether the nickel species is properly supported on a surface;[3b, 6b, 16] and 3) in our hands, the formation of nickel-carbene species **6** in water is instantaneous and **6** remains intact and reactive in water over a long period of time.[11] Although it is unlikely that metal particles form under these conditions,[6b, 17] we tested for surface catalysis versus homogeneous catalysis with Crabtree's mercury drop test. OER catalyzed by **2** did not

respond to mercury drops in the reaction over > 1000 TON (Table 1, entry 3), strongly suggesting a homogeneous reaction. Finke has discussed the validity of the Hg drop test for nickel(II) carboxylates:[18] these appear to be deactivated by reduction by mercury, much like palladium(II).[19] Thus, the reaction passing Finke's first three criteria for homogeneity (appearance, clean kinetics through long conversion, and Hg drop test),[18] we assign this has homogenous. It is most likely that there is a catalyst initiation step that happens rapidly, as we expected for such a high potential stoichiometric oxidant. We have not structurally characterized this initiation and have characterized the active catalytic species. Quantitative poisoning (Finke's fourth test) is not proven in OER, and has not been used, even in controversial cases,[20] so we did not pursue it. Instead, we included periodate in place of CAN to effect the same reaction and observed oxygen evolution, confirming OER reactivity in the absence of cerium oxide particles (Table 1, entry 9). We never encountered any (NHC)Ni complex that has significantly different reactivity from **2** or **3**, which would add some evidence of homogeneity. A reaction of **6** with CAN would provide this, but we found **6** unstable to the CAN conditions. From these combined data, and the fast linear kinetic data that supports saturation catalysis without change in reaction mechanism, we find that the nickel-carbene species most likely retain their natures as homogeneous catalysts under chemical water oxidation conditions and that, while formation of rapidly-activating, mercury-inert heterogeneous nickel-containing particles is possible, it is likely that the observed OER involves homogeneous catalysis.

Table 1. Water oxidation by carbene supported catalysts under chemical conditions[a]

Entry	Catalyst	Time (min)	TON
1	**1**	30	325
2	$[Ir(COD)Cl_2]_2$	30	–[c]
2	**2**	30	381
3[b]	**2**	300	1030 (1155)[d]
4[b]	**3**	300	1057
5	$Ni(acac)_2$	300	–
6	$Ni(acac)_2$ + ligand	300	–
7	imidazole ligand	300	–
8	$NiCl_2$	300	–
9[e]	**2**	30	252

[a] Reaction conditions: 1 mg of catalyst, 2 mL deionized water, 2.0 g CAN, 70 °C. [b] 5.0 g CAN is dissolved in 5 mL H_2O. [c] No gaseous product detected. [d] TON from mercury drop test in parenthesis. [e] 2.0 g sodium periodate is the oxidant instead of CAN. CAN = $[NH_4]_2[Ce(NO_3)_6]$

2.3. Electrochemical Water Oxidation

Since nickel complexes **2** and **3** are prolific homogeneous water oxidation catalysts, we tested their heterogeneous electrochemical reactivity. Electrodes were prepared by mounting **2** or **3** onto a nickel foam surface (Changde Lyrun, 25 cm^2). Imidazole derivatives are known to be effective for coating surfaces from metal electrodes to quantum dots under neutral to basic conditions,[21] so we reasoned that these substructures should be able to link the molecular nickel center to the surface., frequently through a nitrogen atom in an edge-on orientation.[21a] Moreover, imidazole's stability at high positive electrode potentials should allow desirable catalyst stability in electrochemical OER.[22] Accordingly, we functionalized a nickel foam electrode with nickel-carbene species **2** and **3** to effect electrochemical oxygen evolution (Scheme 1). We chose nickel foam as the electrode, because it has useful electrocatalytic characteristics—it does not bottleneck the overall OER kinetics—and maintains suitability for wide adoption. Wet coating of the nickel foam separately enables complexes **2** and **3** to self-assemble a thin, continuous film on the nickel foam electrode while maintaining electronical conductivity of the surface. Under kinetic conditions, the coating of **2** also shows desirable resilience to leaching and stripping compared to those of the nickel species without a binding bridge. In fact, we see almost no leaching or stripping under conditions in which other nickel species we tested quickly stripped away from the electrodes. We made this determination by developing a technique to use ^{31}P NMR line broadening to detect free nickel in solution (section 4.3). Previously such measurements were limited to cobalt.[7b] We propose that, upon interaction with the nickel foam surface, nickel species **2** or **3** most likely forms poly-imidazole bridges to electrode surface, as illustrated in scheme 1. We find this surface-mounted catalyst a more active heterogeneous catalyst than either the homogeneous nickel species or the porous nickel foam electrode.

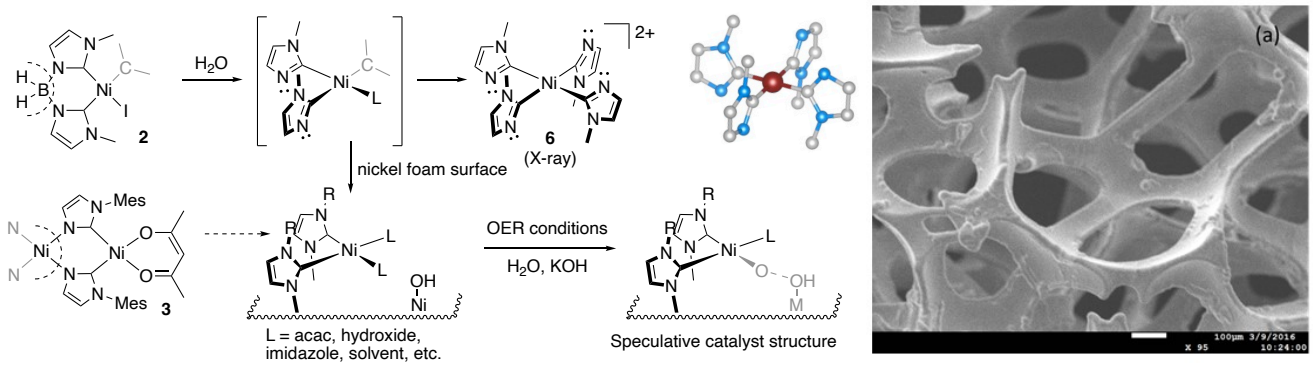

Scheme 1. Left: Speculation for the structure for the surface-supported catalyst bound through imidazole nitrogen atoms. Right: SEM image of nickel foam electrode coated with complex **2**, the latter forming a thin, smooth, and continuous film on the surface. CCDC 1455848 contains supplementary crystallographic data for **6**.

The electrocatalytic activities of **2**- and **3**-coated electrodes were studied in the OER by steady-state polarization, which we found to be the most appropriate experiment for our purposes (Figure 2). The reactivity of bare nickel foam was also studied as a (less reactive) positive control. We note that the onset potentials are very similar for all three electrodes, at ca. 250 mV overpotential, a relatively low overpotential for base metal catalysts. At 20 mA/cm^2 the electrodes coated with **2** and **3** required overpotentials of 350 mV and 330 mV, respectively, while the bare nickel foam demanded a significantly higher overpotential of > 400 mV. Further increasing the overpotential results in very rapid increase of current density for electrodes coated with **2** and **3**, achieving > 40 mA/cm^2 at 400 mV. In contrast, bare nickel foam struggled to reach 30 mA/cm^2 at nearly 500 mV. Fresh electrodes were prepared for each experiment. Trials for assessment of catalyst productivity were replicated through minimally 6 trials. These data show that while commercial porous nickel foam is a reactive OER catalyst, **2**- and **3**-coated electrodes are much more efficient in the OER. This experiment also shows that our coating process effectively modifies the surface of the electrodes, knowing that a partially-coated electrode performs similarly to a bare electrode. Given the low loading of **2** and **3** on the electrodes (as low as ca. 12 μg/cm^2: note that the electrode is large, at 25 cm^2, corresponding to an actual weight difference of 0.3 mg), we are excited to see remarkable specific activity up to 1.6 and 2.6 A/mg at 345 mV overpotential for **2** and **3**, respectively. At each of the potentials measured and at a constant current of 10 mA/cm^2, the potential deviate by less than 1 mV over 10 hours (Figures 2, 3). Thus, OER is the only practical

reaction that can proceed on stoichiometric scale; thus, the product gas was not further characterized (see supporting information regarding using Faradic measurements to track kinetics).[23] In a worst case, reactions of nickel foam and catalysts derived from **2** and **3** are controlled against each other.

Further, the Tafel slopes of 40 mV/decade (for **3**-coated electrode) and 47 mV/decade (for **2**-coated electrode) were observed over more than a decade of current density contrasted with the 72 mV/decade of bare nickel foam (Figure 2, right). These Tafel slopes of **2** and **3** place them among the most efficient water oxidation catalysts including noble-metal catalysts IrO_2 and RuO_2 and the state-of-the-art base-metal catalysts (30-60 mV/decade).[24] The low values of Tafel slope of both **2**- and **3**-coated electrodes suggest that these materials allow a lower activation barrier for O–O bond formation through a novel molecular mechanism, compared to simple nickel oxides.

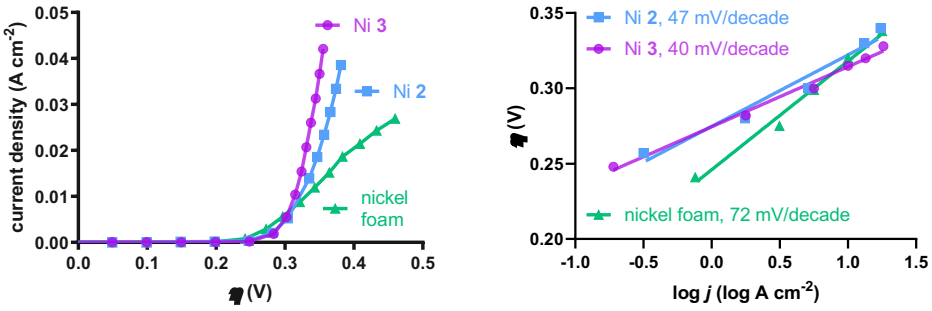

Figure 2. Left: steady-state polarization data for oxygen evolution in 30 wt% potassium hydroxide showing electrodes coated with **2**, **3**, and bare nickel-foam. Overpotential is calculated as the difference between the applied potential and the reversible electrode potential for oxygen evolution in 30% potassium hydroxide. Right: Tafel plots for electrodes coated with catalysts **2**, **3**, and the bare nickel foam electrode.

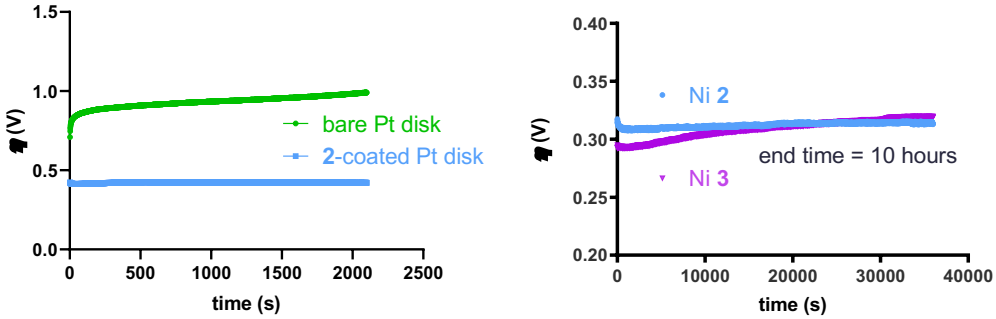

Figure 3. Left: galvanostatic test of **2**-coated platinum electrode at 10 mA/cm^2 in 30 w/v% potassium hydroxide at 25 °C. Right: stress test of **2**- and **3**-coated nickel foam electrodes at 10 mA/cm^2 in 30 w/v% potassium hydroxide at 25 °C monitored for 10 hours.

The remarkable catalytic reactivity shown in figure 2 must originate nickel species from **2** and **3**, not the nickel foam, because the distinct current-overpotential profiles and Tafel slopes are evidence for effective surface modification by surface coating. To further support this point, we coated **2** onto a platinum electrode and observed the coating to enhance the activity of platinum significantly, platinum being an inefficient electrocatalyst for OER (Figure 3, left). At 10 mA/cm^2, the oxygen evolution overpotential on the **2**-coated electrode was ca. 0.5 V lower than a bare platinum disk electrode.

This surface derivatization of nickel foam electrode and platinum disk electrode most likely retains the nickel-carbene moiety as the WOC rather than forming nickel oxide particles because 1) we do not observe particle formation or oxide growth in the SEM of the foam electrodes (see supporting information), and 2) the galvanostatic profile of the **2**-coated platinum electrode is flat throughout the test and did not show an initiation phase for particle formation while the electrode potential is recorded every second (Figure 3, left).[25] In fact, **2** and **3** form stable layers on the electrode surface. For example, when nickel foam electrodes are coated by **2** and **3**, we observe stable OER for hours, much like their homogeneous counterparts. In a stress test on **2**- and **3**-coated electrodes at 10 mA/cm^2 over 10 hours (Figure 3, right), the rate of change of electrode potential over the 10 hours was small (0.2 μV/sec for **2** and 0.8 μV/sec for **3**, or only ca. 2% degradation for **2** and 8% for **3** over 10 hours), demonstrating useful robustness for electrochemical OER.

2.4. Mechanistic Discussion

We believe the high reactivity of **2** and **3** as water oxidation catalysts originates from formation of an active catalyst resulting from combination of the nickel foam with the added soluble nickel complex, although we have not characterized the structure of this active species. Some qualitative data that describe this species are available from XPS and Raman studies. We found X-ray photoelectron spectroscopy (XPS) to be a useful tool to determine the composition of **2**- or **3**-coated nickel foam electrodes, as it provides evidence for the proposed nickel-carbene functionality persisting throughout an OER (Figure 4). Prior to OER use, nickel atoms were characterized by $2p_{3/2}$ peaks, and peaks appeared at energies consistent with nickel in both the +2 and 0 oxidation states. Oxygen was detected by its 1s peaks, which appear most consistent with oxides (529.5 eV), and sp^3-hybridized oxygen (531.4 eV), which indicates hydroxide ligands. The nitrogen 1s peaks at 399.5 eV and 401.0 eV represent the nitrogen atoms in the imidazolium ring in the deposited nickel complex. We also observe an iodine peak, which appears to arise from the Ni—I bond in the structure of **2** (see supporting information). While adventitious carbon is observed at 285.0 eV, the shoulder peak at 288.5 eV is appropriate for *N*-heterocyclic carbenes metal complexes as demonstrated in various examples.[26] We detect no boron in this data set, which is consistent with our surface-binding hypothesis in which the cleavage of the boron moiety is facile (Scheme 1). Data arising from complexes **3** give highly analogous findings to those from **2** and are shown in the Supporting Information. We searched for signals appropriate for iron in the survey scans for each XPS experiment but found none. As Boettcher points out,[27] trace iron in the nickel foam could substantially modify our experimental findings. While trace iron could be present, we were unable to detect it by XPS.

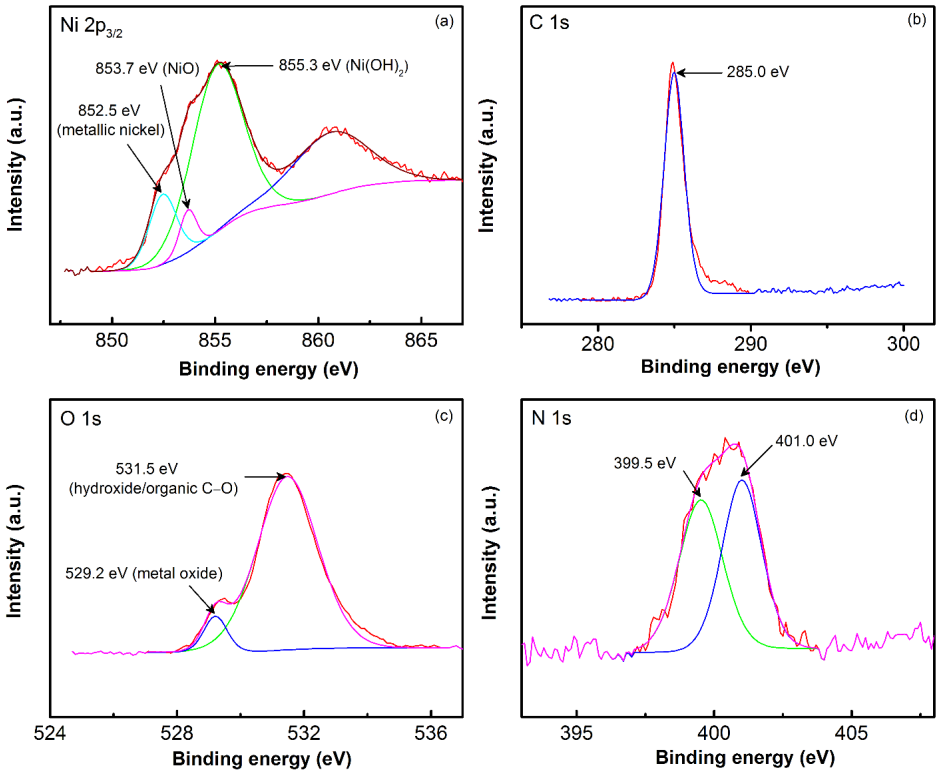

Figure 4. Binding energy of nickel $2p_{3/2}$ (a), carbon 1s (b), oxygen 1s (c), and nitrogen 1s (d) for **3** in the as-prepared state. XPS data for **2**, which also show iodine 3d, are illustrated in figure S5.

We re-examined our electrodes using XPS techniques after the electrodes had been subjected to OER experiments (Figure 5). We find only a small amount of nickel oxide signal, whereas the oxygen 1s peaks suggested that an increase of the hydroxide on the surface. Thus, the OER test in potassium hydroxide aqueous solution transforms the surface into a more hydrated structure. Importantly, the imidazole nitrogen signal remains in the electrode after OER, showing persistence of the carbene fragments. The nitrogen XPS signal is not strong after reaction. However, it appears at the same binding energy as the starting sample and it is accompanied by a carbon at the same binding energy as the starting catalyst. The catalyst had operated over 10 hours before we acquired the after-reaction data, and we did not expect a strong nitrogen signal, especially as nitrogen is not as easily detected by XPS as other nucleii. In contrast to the N1s peaks before OER, only one broad peak matching with C—N bonds at 400.9 eV was found for the electrochemically treated sample, suggesting a more symmetrical structure of the imidazole ligand, possibly through ligand "L" substitution by a hydroxide at the mounted nickel center (Scheme 1). Carbon data confirms

the persistence of our apparent imidazolium carbene species at 288.5 eV with the introduction of potassium (293.3, 296.1 eV) from KOH. Data for a **3**-coated electrode, shown in Supporting Information, is highly analogous to the **2**-coated electrode. The XPS data reassure us that the active catalyst involves a nickel-carbene structure, wherein the imidazole groups are most probably anchored to the electrode surface.

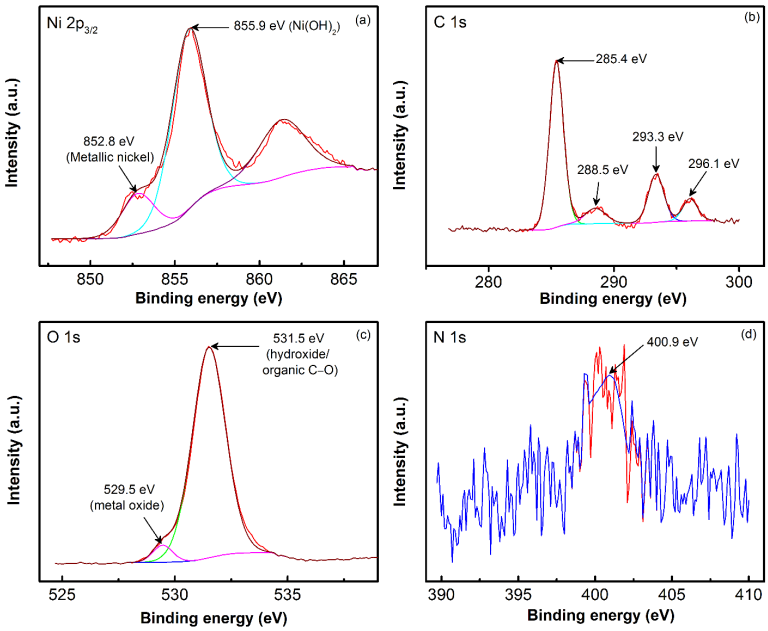

Figure 5. Binding energy of nickel 2p (a), carbon 1s (b), oxygen 1s (c), and nitrogen 1s (d) for **3** after OER activity test. XPS data for **2**, which also show iodine 3d, are illustrated in Supporting Information.

Furthermore, we performed surface Raman experiments in which we observe a persistent single peak at near 2850 cm^{-1} (see supporting information figure S8), appropriate for imidazole C—N(symmetrical) bond in a metal-carbene structure.[28]

With all the data consistent with a persistent nickel-carbene catalyst, we reason that the origin of the catalytic activity of our system is the unique donor ability of the carbene ligand that remains part of the catalyst throughout the OER. Other ligands on nickel in the initial surface coordination complex (L in Scheme 1) could be acetylacetonate (from **3**), iodide, imidazole (from **2**), solvent, or hydroxide. Quickly upon the initiation of oxygen evolution in aqueous solutions, the groups “L”

in scheme 1 are likely replaced with hydroxide ligands. We interpret our Tafel slopes of 40 and 47 mV/decade to be consistent with a Ni^{II}/Ni^{III} couple.[50] Therefore we believe that electrooxidation of a nickel hydroxide is promoted by the strongly donating carbene ligands, forming an electrophilic oxygen center that engages in bonding with another nickel hydroxide group, as sketched in scheme 1. We perceive that our structurally-unique carbene ligands enable this process by 1) facilitating the Ni^{II}/Ni^{III} oxidation at the C-ligated nickel center and 2) weakening the Ni—O bonds trans to the strong-field ligands.

3. Conclusions

We report the first homogeneous nickel water oxidation catalysts that can be anchored on metal-electrode surface to enable high current densities with an excellent efficiency and low overpotential while retaining high stability in heterogeneous electrolysis. These nickel catalysts show reactivities abreast of the best base-metal catalysts for OER, both in homogeneous chemical catalysis literature and in the heterogeneous electrochemical literature. Our data support robust and effective modification of both nickel-electrode and platinum-electrode surfaces, forming highly active heterogeneous catalysts comprising bound carbene-nickel(II) centers. We propose that these bound carbene-nickel(II) species are the active catalysts for the observed OER and those donor carbene ligands can account for the facilitated molecular mechanism of O—O bond formation. The insight into the molecular structure of the nickel catalysts, as well as our strategy of preparing stable, surface-supported catalysts using imidazole carbene complexes, are likely to motivate more interesting discoveries in this field.

4. Experimental

4.1. General Procedures

All air and water sensitive procedures were carried out either in a Vacuum Atmosphere glove box under nitrogen (2-10 ppm O_2 for all manipulations) or using standard Schlenk techniques under nitrogen. Tetrahydrofuran is purchased from VWR and dried in a J. C. Meyer solvent purification system with alumina/copper(II) oxide columns. High purity water (18.2 Mohm-cm,

4 ppb total organic carbon) is used throughout this project. Iridium complex **1** was synthesized using a previously reported method.[10] Nickel complexes **2** and **3** were synthesized following reported procedures.[11] Nickel foam was acquired from Changde Lyrun (China) with the geometric area of the active electrode was 25 cm^2. A mercury/mercuric oxide (MMO) is used as a reference electrode (in a 30 w/v % potassium hydroxide aqueous solution, EMMO = ENHE + 0.098 V) and a nickel mesh is used as the counter electrode. The electrolyte is 30 w/v % aqueous potassium hydroxide solution. Same concentration of potassium hydroxide solution is used for both the reference electrode and the electrolyte to avoid the development of a liquid junction potential.

Scanning Electron Microscopy (SEM) were conducted using instrument model JEOL JSM-7001 microscope at an operating voltage of 200 kV, equipped with a Gatan Orius CCD camera. Surface oxidation states were identified by X-ray-Photoelectron Spectroscopy (XPS) measurements were made using Kratos AXIS Ultra spectrometer. Raman spectra were measured with Horiba XploRA Raman Microscope System with both visible and near-IR detectors.

4.2. Oxygen Evolution under Chemical Oxidation Conditions

In a typical reaction, various amounts of iridium or nickel complex (1.3 μmol (carbene)metal loading) and cerium ammonium nitrate (CAN, 2.0 g, 3.6 mmol, 2800 equiv. per metal atom) are dissolved in deionized water (2.0 mL) in a 25 mL round bottom flask. The reaction flask is wrapped in aluminum foil to eliminate potential photochemical reactivity. The reaction is then heated in an oil bath to the temperature specified in the main text and stirred on a standard stir place (ca. 100 rpm) and gas evolution is measured by eudiometry, with oxygen collected over water in a 1 L graduated cylinder.

The gas volume is corrected for water vapor content and atmospheric pressure (by leveling water levels before reading) and controlled against catalyst-free, otherwise identical runs. The experiment setup is drawn in detail in the figure S1. In the case of the mercury drop test, liquid mercury was added to one of two reactions, prepared as above once the catalyst was initiated. No deviation in reactivity was observed.

4.3. Immobilization of Nickel Complexes

A macroporous nickel foam with a density of 420 g/m^2 and thickness of 2.2 mm provides a high surface area to host the nickel complexes. The geometric area of the electrode is large, at 25 cm^2 with a 5 cm x 5 cm cross section. The pores ranged from 500 to 800 microns. Nickel complex **2** or **3** is dissolved in a solution of 1% water in THF. The aforementioned nickel foam is aged in the assembling solutions of **2** or **3** for 3 hours before it is removed from the solution and dried in an oven at 30 ^{o}C for 2 hours. Any excess, unbound nickel is then washed away with a gently flow of deionized water. The foam is again put in a drying oven at at 30 ^{o}C for overnight. The loading mass of the nickel complexes can be calculated from the difference of the nickel foam before and after this treatment. We find this method reliable and reproducible, consistently loading ca. 12 μg nickel complex **2** per cm^2 onto the electrode. A structural diagram for the product is sketched in figure S2.

4.3. Leaching and Stripping Test

Some transition metals are known to induce ^{31}P line broadening.[29] We found nickel complex **2** and several other nickel(II) species to also induce line broadening of the peak of 10.0 mg PPh_3 in THF-d_8 in ^{31}P NMR. We are able to establish a linear relationship between the concentration of nickel(II) **2** in solution and linewidth of the PPh_3 peak (Figure S3). When testing the efficiency of wet loading of nickel species onto electrodes, and the degree nickel(II) is leached or stripped from electrodes, we measured the nickel(II) concentration by converting ^{31}P NMR linewidth to its corresponding concentration value. Typically, we put coated electrodes under vigorous stirring in 30% KOH solution to trigger leaching and stripping and monitor the process overtime. Under our kinetic conditions, most nickel(II) species see significant leaching and stripping, while Ni **2** stays stably bound to the electrode (Figure 6).

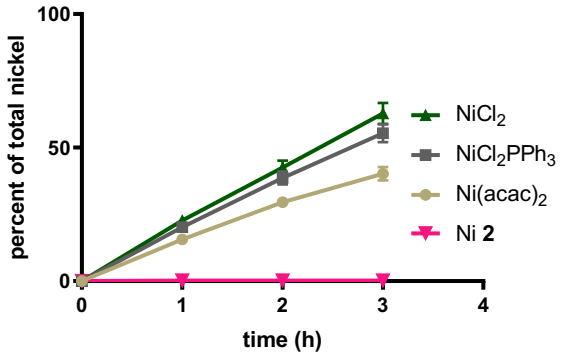

Figure 6. Leaching and stripping of nickel(II) species from loaded electrodes over time. Leaching of Ni **2** is not statistically significant (95% likelihood of zero leaching and stripping).

4.4. Electrochemical Measurements

Steady state potentiostatic polarization measurements were carried out by holding the electrode potential for 15 minutes at each chosen value of potential step. Using the steady-state polarization technique instead of linear sweep voltammetry we ensured that slow changes to the surface chemistry did not interfere with the accurate determination of the kinetic parameters. All the electrode potentials have been reported after correcting for potential drop due to uncompensated solution resistance between the working and reference electrodes. Typically, the experiments were performed at 25 ^{o}C.

4.5. XPS Measurements

The electrode foam immobilized with nickel complexes are studied under XPS both before and after OER. While the measurements coming from a sample based on **3** are reported in figures 4 and 5 above, respectively collected before and after OER experiments. We also report analogous XPS data measured for electrode with **2**; these are shown in figures S5 and S6. These differ from those of **3** in that the nitrogen signal is very weak after electrolysis. Figure S7 shows XPS data for iodine before and after OER. The iodine ligand of **2** remains associated with the catalyst before and after electrolysis. As expected, it is evident that iodide is oxidized to iodate under the OER conditions.

4.5. Galvanostatic Test on Platinum Disk

Galvanostatic measurements were carried out on a Pt disk electrode coated or not coated with catalyst **2**. The diameter of the Pt disk electrode is 5 mm. The galvanostatic experiments were run at 10 mA/cm^2 (2 mA in total) in 5.35 M KOH solution and the electrode potential was monitored for 2100s. Mercury/mercury oxide was used as reference electrode and Pt wire as counter electrode. Typically, the experiments were performed at 25 ^{o}C.

Acknowledgments

This work was sponsored by the National Science Foundation (CHE-1856395), the Hydrocarbon Research Foundation and the Loker Hydrocarbon Research Institute. We thank the NSF (DBI-0821671, CHE-0840366, CHE-1048807) and NIH (1 S10 RR25432) for sponsorship of research instrumentation.

Supporting Information

The Supporting Information is available free of charge at: xxx.
Supplemental diagrams, XPS data, microscope images, and Raman spectra (PDF)

5. References

[1] (a) J. D. Blakemore, R. H. Crabtree, G. W. Brudvig, *Chem. Rev.* 115 (2015) 12974–13005. (b) X. Zou, Y. Zhang, *Chem. Soc. Rev.* 44 (2015) 5148–5180. (c) B. M. Hunter, H. B. Gray, A. M. Müller, *Chem. Rev.* 116 (2016) 14120–14136.
[2] K. S. Joya, Y. F. Joya, K. Ocakoglu, R. Van De Krol, *Angew. Chem. Int. Ed.* 52 (2013) 10426–10437.
[3] (a) A. R. Parent, K. Sakai, *ChemSusChem* 7 (2014) 2070–2080. (b) A. Singh, L. Spiccia, *Coord. Chem. Rev.* 257 (2013) 2607.
[4] (a) S. M. Barnett, K. I. Goldberg, J. M. Mayer, *Nat. Chem.* (2012)4 498–502. (b) M. T. Zhang, Z. Chen, P. Kang, T. J. Meyer, *J. Am. Chem. Soc.* 135 (2013) 2048–2051. (c) Z. Chen, T. J. Meyer, *Angew. Chem. Int. Ed.* 52 (2013) 700–703.
[5] (a) J. Guan, Z. Duan, F. Zhang, S. D. Kelly, R. Si, M. Dupuis, Q. Huang, J. Q. Chen, C. Tang, C. Li. *Nat. Catal.* 1 (2018) 870–877. (b) D. M. Robinson, Y. B. Go, M. Mui, G. Gardner, Z. Zhang,

D. Mastrogiovanni, E. Garfunkel, J. Li, M. Greenblatt, G. C. Dismukes, *J. Am. Chem. Soc.* 135 (2013) 3494–3501. (c) G. Maayan, N. Gluz, G. Christou, *Nat. Catal.* 1 (2018) 48–54.
[6] (a) W. C. Ellis, N. D. McDaniel, S. Bernhard, T. J. Collins, *J. Am. Chem. Soc.* 132 (2010) 10990–10991. (b) J. L. Fillol, Z. Codolà, I. Garcia-Bosch, L. Gómez, J. J. Pla, M. Costas *Nat. Chem.* 3 (2011) 807–813. (c) D. Mitra, P. Trinh, S. Malkhandi, M. Mecklenburg, S. M. Heald, M. Balasubramanian, S. R. Narayanan. *J. Electrochem. Soc.* 165 (2018) F392–F400. (d) D. Mitra, S. R. Narayanan. *Top. Catal.* (2018) 61 591–600.
[7] (a) Q. Yin, J. M. Tan, C. Besson, Y. V. Geletii, D. G. Musaev, A. E. Kuznetsov, Z. Luo, K. I. Hardcastle, C. L. Hill, *Science* 328 (2010) 342–345. (b) S. J. Folkman, J. Soriano-Lopez, J. R. Galán-Mascarós, Finke, R. G. *J. Am. Chem. Soc.* 140 (2018) 12040–12055. (c) M. Blasco-Ahicart, J. Soriano-Lopez, J. J. Carbo, J. M. Poblet, J. R. Galan-Mascaros, *Nat. Chem.* 10 (2018) 24–30. (d) Lv, H. J. Song, Y. V. Geletii, J. W. Vickers, J. M. Sumliner, D. G. Musaev, P. Kögerler, P. F. Zhuk, J. Bacsa, G. Zhu, C. L. Hill, *J. Am. Chem. Soc.* 136 (2014) 9268–9271.
[8] (a) M. Zhang, M. T. Zhang, C. Hou, Z. F. Ke, T. B. Lu, *Angew. Chem. Int. Ed.* 53 (2014) 13042–13048. (b) J. Hessels, E. Masferrer-Rius, F. Yu, R. J. Detz, R. J. M. Klein Gebbink, J. N. H. Reek, ChemSusChem 13 (2020) 6629–6634.
[9] S. Kaufhold, L. Petermann, R. Staehle, S. Rau, *Coord. Chem. Rev.* 304–305 (2015) 73–87.
[10] (a) J. J. A. Celaje, Z. Lu, E. A. Kedzie, N. J. Terrile, J. N. Lo, T. J. Williams, *Nat. Commun.* 48 (2016) 829–834. (b) Z. Lu, Williams, T. J. *Chem. Commun.* 50 (2014) 5391–5393. (c) Z. Lu, V. Cherepakhin, I. Demianets, P. J. Lauridsen, T. J. Williams, *Chem. Commun.* 54 (2018) 7711–7724. (d) Z., Lu, I., Demianets, R., Hamze, N. J. Terrile, T. J. Williams, *ACS Catal.* 6 (2016) 2014–2017. (e) Z. Lu, V. Cherepakhin, T. Kapenstein, T. J. Williams, *ACS Sustain. Chem. Eng.* 6 (2018) 5749–5753. (f) V. Cherepakhin, T. J. Williams, *ACS Catal*. 8 (2018) 3754-3763. (g) V. K. Do, N. Alfonso Vargas, A. J. Chavez, L. Zhang, V. Cherepakhin, Z. Lu, R. P. Currier, P. A. Dub, J. C. Gordon, T. J. Williams, *Catal. Sci. Technol*. 12 (2022) 7182-7189
[11] Z. Lu, Williams, T. J. *ACS Catal.* 6 (2016) 6670–6673.
[12] (a) I. Corbucci, A. Petronilho, H. Müller-Bunz, L. Rocchigiani, M. Albrecht, A. Macchioni, *ACS Catal.* 5 (2015) 2714–2718. (b) R. Lalrempuia, N. D. McDaniel, H. Müller-Bunz, S. Bernhard, M. Albrecht, *Angew. Chem. Int. Ed.* 49 (2010) 9765–9768.
[13] Zhao, Y. et al. *Proc. Natl. Acad. Sci*. 115 (2018) 2902–2907.
[14] (a) J. F. Hull, D. Balcells, J. D. Blakemore, C. D. Incarvito, O. Eisenstein, G. W. Brudvig, R. H. Crabtree, *J. Am. Chem. Soc.* 131 (2009) 8730–8731. (b) D. B. Grotjahn, D. B. Brown, J. K. Martin, D. C. Marelius, M.-C. Abadjian, H. N. Tran, G. Kalyuzhny, K. S. Vecchio, Z. G. Specht, S. A. Cortes-Llamas, V. Miranda-Soto, C. van Niekerk, C. E. Moore, A. L. Rheingold, *J. Am. Chem. Soc.* 133 (2011) 19024–19027. (c) Specifically regarding the utility of CAN for comparing disparate OER catalysts, see L. Duan, F. Bozoglian, S. Mandal, B. Stewart, T. Privalov, A. Llobet, L. Sun, *Nat. Chem.* (2012) 4 418–423
[15] E. G. Gori, G. L. Petriconi, H. M. Papée, *Pure Appl. Geophys. PAGEOPH* 72 (1969) 307–314.
[16] X. Zhou, T. Zhang, C. W. Abney, Z. Li, W. Lin, *ACS Appl. Mater. Interfaces* 6 (2014) 18475–18479.
[17] M. S. Tsai, *J. Cryst. Growth* 274 (2005) 632–637.
[18] J. A. Widegren, R. G. Finke, *J. Mol. Catal. A: Chem*. 198 (2003) 317–341.

[19] (a) O. N. Gorunova, I. M. Novitskiy, Y. K. Grishin, I. P. Gloriozov, V. A. Roznyatovsky, V. N. Khrustalev, K. A. Kochetkov, V. V. Dunina, *Organometallics* 37 (2018) 2842–2858. (b) I. C. Chagunda, T. Fisher, M. Schierling, J. S. McIndoe. *Organometallics* 42 (2023) 2938–2945.
[20] J. W. Vickers, H. Lv, J. M. Sumliner, G. Zhu, Z. Luo, D. G. Musaev, Y. V. Geletii, C. L. Hill. *J. Am. Chem. Soc.* 135 (2013) 14110–14118.
[21] (a) P. Cao, R. Gu, Z. Tian, *J. Phys. Chem. B* 107 (2003) 769–777. (b) Z. Zhang, S. Chen, Y., Li, S. Li, L. Wang, *Corros. Sci*. 5 (2009) 291–300. (c) P . Zhang, S. Liu, D. Gao, D. Hu, P. Gong, Z. Sheng, J. Deng, Y. Ma, L. Cai *J. Am. Chem. Soc*. 134 (2012) 8388–8391. (d) E. Petryayeva, U. J. Krull, *Langmuir* 28 (2012) 13943–13951.
[22] H. Rong, M. Xu, Y. Zhu, B. Xie, H. Lin, Y. Liao, L Xing, W. Li *J. Power Sources* 332 (2016) 312–321.
[23] P.A. Kempler, A. C. Nielander *Nat. Commun.* 14 (2023) 1158.
[24] Z.-F. Huang, J. Song, Y. Du, S. Xi, S. Dou, J. M. V. Nsanzimana, C. Wang, Z. J. Xu, X. Wang *Nat. Energy* 4 (2019) 329-338. (b) K. Fan, H. Chen, Y. Ji, H. Huang, P. M. Claesson, Q. Daniel, B. Philippe, H. Rensmo, F. Li, Y. Luo, L. Sun *Nat. Commun.* 7 (2016) 1–9. (c) R. D. L. Smith, M. S Prévot, R. D Fagan, Z. Zhang, P. A Sedach, M. K. J. Siu, S. Trudel, C. P Berlinguette *Science* 340 (2013) 60–63. (d) R. D. L. Smith, M. S. Prévot, R. D. Fagan, S. Trudel, C. P. Berlinguette, *J. Am. Chem. Soc.* 135 (2013) 11580–11586. (e) Y. Liu, Y. Han, Z. Zhang, W. Zhang W. Lai, Y. Wang, R. Cao. *Chem. Sci.* 10 (2019) 2613-2622. (f) M. S. A.; Akbari, Z.; Zand, P.; Aleshkevych, Z. Jagličić, Z. M. M. Najafpour, *Inorg. Chem*. 61 (2022) 3801–3810. (g) for a review, see L.-H. Zhang, S. Mathew, J. Hessels, J. N. H. Reek, F. Yu. *ChemSusChem* 14 (2021) 234-250.
[25] L. A. Stern, L. Feng, F. Song, X. Hu, *Energy Environ. Sci.* 8 (2015) 2347–2351.
[26] (a) L. Jiang, B. Zhang, G. Médard, A. P. Seitsonen, F. Haag, F. Allegretti, J. Reichert, B. Kuster, J. V. Bartha, A. C. Papageorgiou, *Chem. Sci.* 8 (2017) 8301–8308. (b) P. Aydogan Gokturk, S. E. Donmez, B. Ulgut, Y. E. Türkmen, S. Suzer, *New J. Chem.* 41 (2017) 10299–10304.
[27] L. Trotochaud, S. L. Young, J. K. Ranney, S. W. Boettcher, *J. Am. Chem. Soc.* 136 (2014) 6744–6753.
[28] V. O. Santos, M. B. Alves, M. S. Carvalho, P. A. Z. Suarez, J. C. Rubim, *J. Phys. Chem. B* 110 (2006) 20379–20385.
[29] S. J. Folkman, J. Soriano-Lopez, J. R. Galán-Mascarós, R. G. Finke, *J. Am. Chem. Soc.* 140 (2018) 12040–12055.

Supporting Information for

An Immobilized (Carbene) Nickel Catalyst for Water Oxidation

Zhiyao Lu, Debanjan Mitra, Sri R. Narayan, and Travis J. Williams*

Donald P. and Katherine B. Loker Hydrocarbon Institute, Wrigley Institute of Environment and Sustainability, and Department of Chemistry
University of Southern California
837 Bloom Walk, Los Angeles, California, 90089-1661, United States

Travis J. Williams: travisw@usc.edu

Table of Contents

General Procedures

Diagrams of apparatus and structures

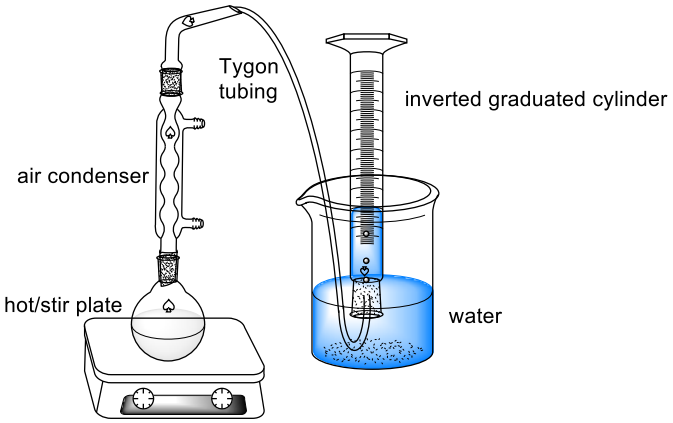

Figure S1. Apparatus for OER under chemical oxidation conditions.

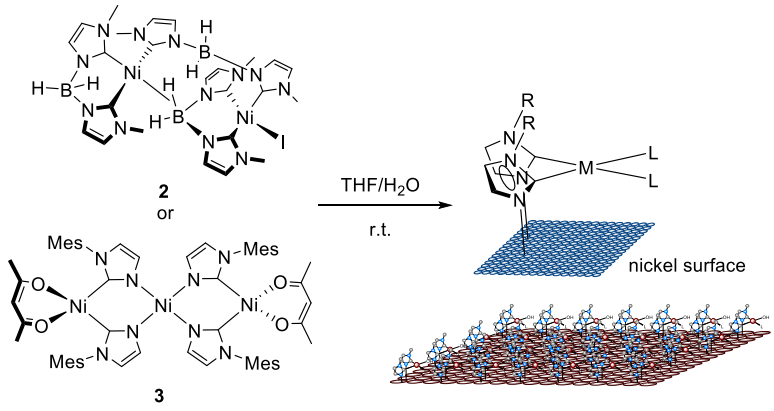

Figure S2. Structural Diagram of Catalyst Immobilization

Leaching and stripping test

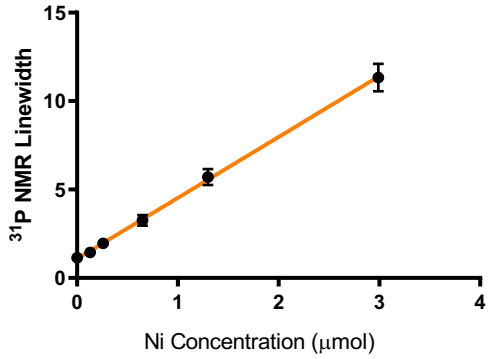

Figure S3. Standard curve of nickel(II) concentration in solution versus ^{31}P NMR peak linewidth.

SEM Images

Immobilized nickel catalysts were observed under SEM showing macroporous structure of the electrode. No significant difference has been observed for the foam before and after the OER. We conclude the immobilized nickel forms a very thin film that is contiguous across the nickel foam surface.

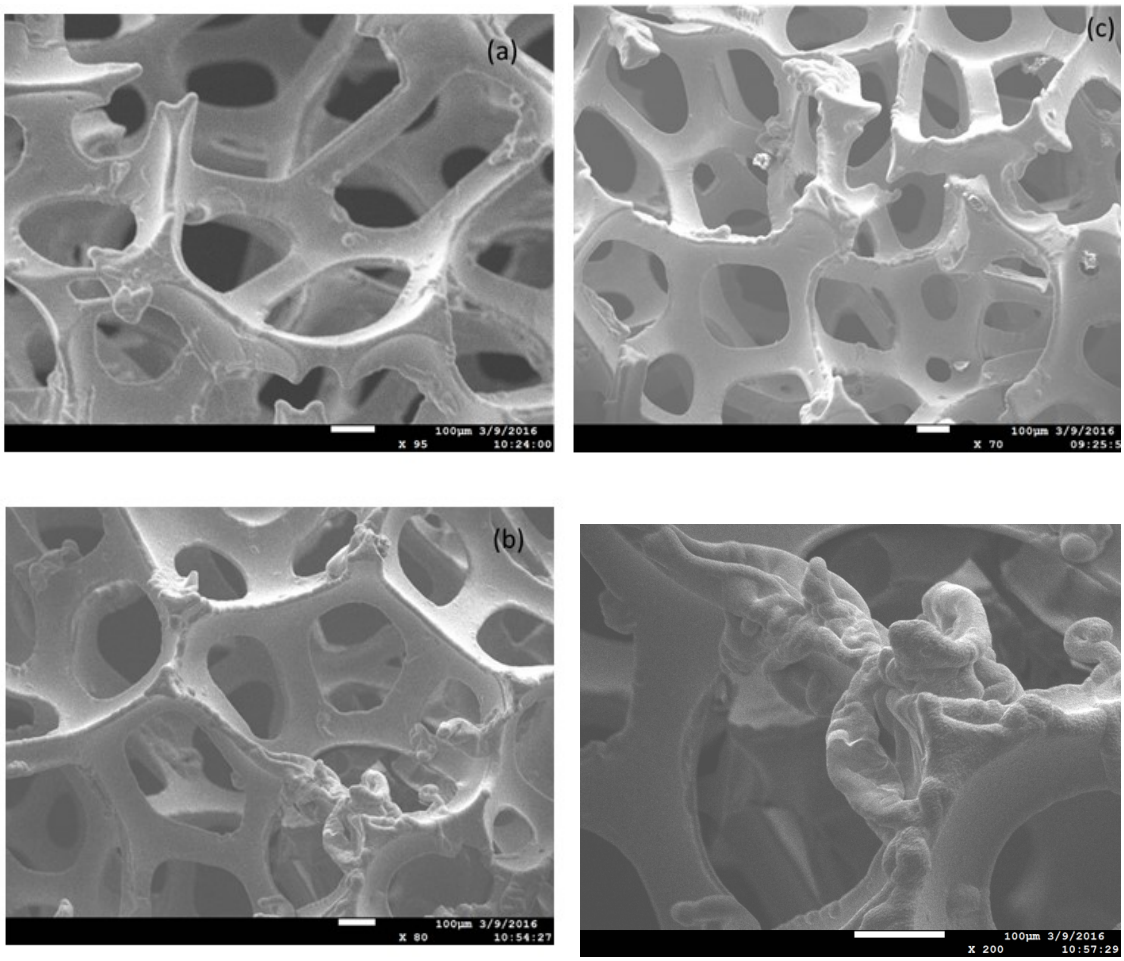

Figure S4. SEM images of electrodes before OER: **2**-coated nickel foam (top left), **3**-coated nickel foam (top right). Images of electrodes after OER: **2**-coated nickel foam electrode (bottom left), **3**-coated nickel foam electrode (bottom right).

XPS Data for 2

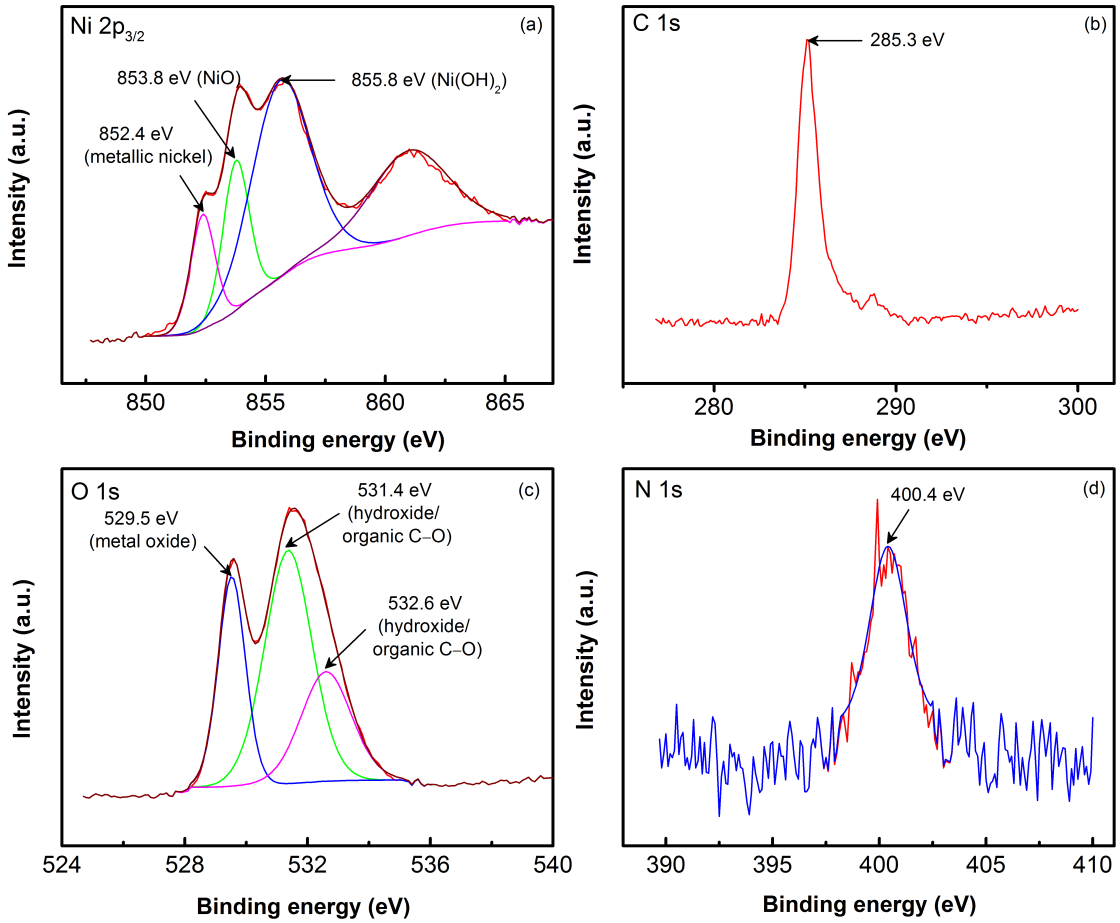

Figure S5. Binding energy of nickel $2p_{3/2}$ (a), carbon 1s (b), oxygen 1s (c), and nitrogen 1s (d) for **2** in the as-prepared state.

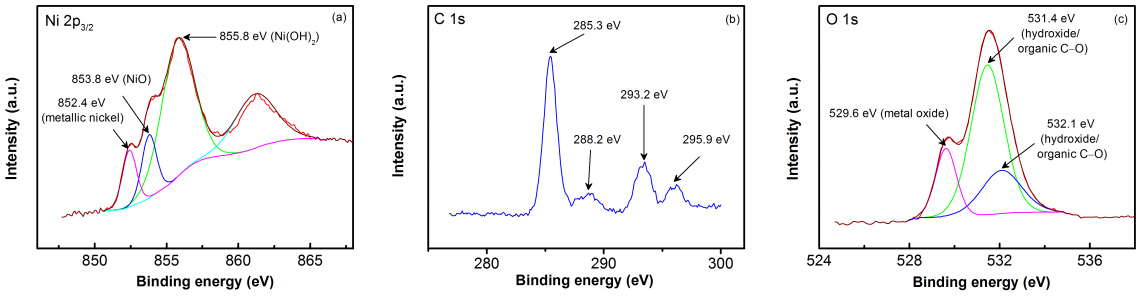

Figure S6. Binding energy of nickel 2p (a), carbon 1s (b), and oxygen 1s (c) for **2** after OER activity test.

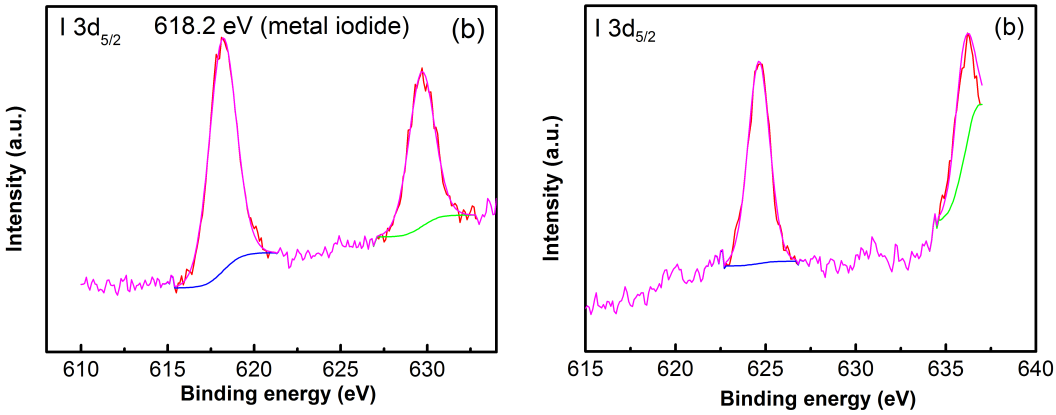

Figure S7. High-resolution XPS spectra showing binding energy of iodine 3d, before (left) and after (right) the OER.

Raman Spectra

Nickel foam coated with catalyst **2** were measured by a Raman microscopy system before and after the OER run. The only distinguishable peak for the surface organic residue was found near 2850 cm^{-1}. Due to the difficulties in sample preparation and experimentation, the intensities do not reflect the relative concentrations.

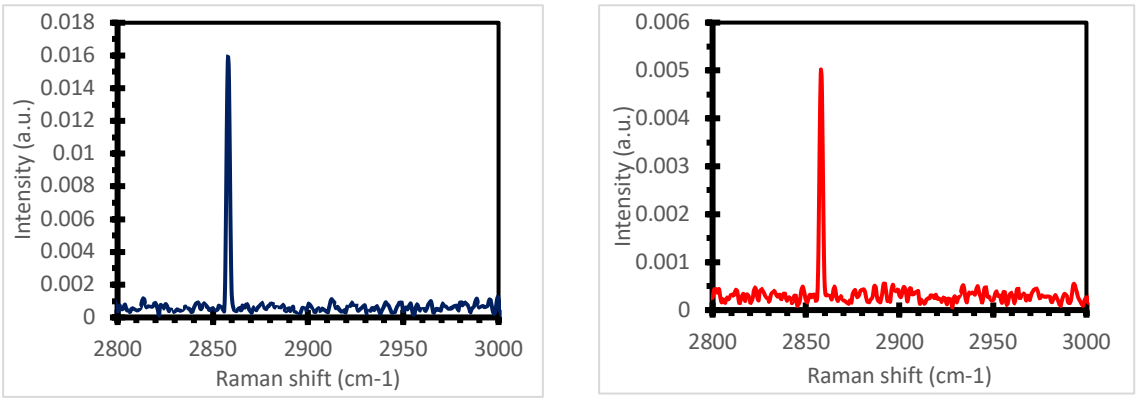

Figure S8. Raman spectra of nickel foam electrode coated with **2** before OER (left) and after OER (right).

To help better understand these spectra, we formulated a catalyst based on coating a gold disk with compound 3 and repeating the experiment above. We saw an analogous peak at 2858 cm-1 that persisted through steady state catalysis (figure S9) at potentials from 400 to 700 mV (v Hg/HgO, figure S10). We were unable to assign or observe post-reaction other peaks in the starting Raman spectrum.

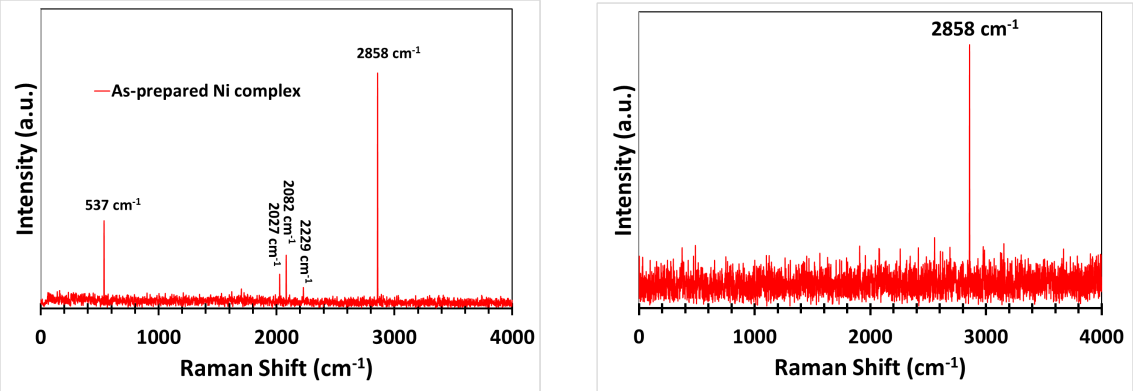

Figure S9. Raman spectra of gold disk electrode coated with **3** before OER (left) and after OER (right).

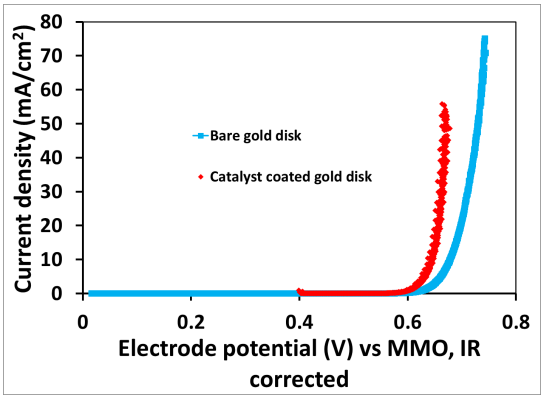

Figure S10. Steady state current vs. potential for OER with a **3**-modified gold disk.

Comment on Faradic Measurements to Track Kinetics

Kempler provides criteria for when Faradaic measurements can be used as a tool to quantify product in OER reactions.[1] Our analysis thereof for our case follows.

- Could multiple products be formed at the applied potential at the working electrode?

  We see no reasonable stoichiometric process that can compete with OER.

- Are reactants/contaminants present in the cell environment (e.g., O_2) that are competitive as defined by the applied potential at the working electrode?

  We see no reasonable reducing agent that could be responsible for a stoichiometric reaction.

- Are all components of the electrocatalyst and its support (carbon is of particular concern for OER) stable at the applied potentials and in the presence of other possible reactants and products (e.g., O_2, H_2O_2, or H^+)?

  All components are stable to the potentials described. We do not add peroxide or acid, and we see that the system is stable to all of the components that we add. We have shown that our

[1] Kempler P.A.; Nielander, A. C. Reliable Reporting of Faradaic Efficiencies for Electrocatalysis Research. *Nat. Commun.* 14 (2023) 1158.

(carbene)nickel functionality is stable to protic environments in reference 11. Nickel foam is well known to be stable to hydroxide solutions.